# Morphological and Crystallinity Studies of Nanofiber Cellulose Based on *Sargassum* sp. Using Multistep Preparation

Nurhayati Nurhayati<sup>1,2,3</sup>, Hari Eko Irianto<sup>2,3,4</sup>, Mochamad Chalid<sup>1,5</sup>, and Rini Riastuti<sup>1\*</sup>

#### \* Corresponding author:

tel: +62-818125159 email: rini.riastuti@ui.ac.id

Received: January 27, 2025 Accepted: May 7, 2025

DOI: 10.22146/ijc.104211

**Abstract:** This study aims to investigate the crystallinity and morphological characteristics of cellulose nanofibers (CNF) isolated from Sargassum seaweed through a multistep preparation. The isolation was conducted in stages, including alkalinization, bleaching, and mechanical reduction in fiber size. In addition to observing the outcomes at each isolation stage, three mechanical processes were implemented to generate CNF. The observed parameters included fiber morphology analyzed using scanning electron microscopy (SEM) and fiber crystallinity tested using X-ray diffraction (XRD). The results indicated that Sargassum mostly exhibits a type  $I\alpha$  structure of cellulose. The multistep treatment, combined with mechanical processing, resulted in finer fibers and an improved crystallinity index, reaching a maximum value of 70.39%. These findings suggest that cellulose nanofibers from Sargassum have the potential to be used in sustainable biomedical materials.

Keywords: Sargassum sp.; cellulose nanofiber; multistep preparation

#### **■ INTRODUCTION**

The utilization of biomass-based materials in various fields is progressively increasing with eco-friendly and sustainable technology improvements. Cellulose is a biopolymer consisting of β-D-glucose units interconnected by  $\beta$ -(1 $\rightarrow$ 4) glycosidic linkages, prevalent in terrestrial plants [1], algae [2], and bacteria [3]. Its abundant availability, biocompatibility, and natural biodegradability make cellulose highly utilized in various industries, including textiles, paper, pharmaceuticals, packaging, and biomedicines [4-5]. The increasing demand for cellulose has intensified the search for promising raw material sources that do not compete with food resources. As an abundant marine biomass resource, seaweed is a promising candidate for cellulose production [6-8]. Research on cellulose extraction from various seaweed species has been widely reported, including green algae [9-11], red algae [8,10,12], and brown algae [8,10,13]. Cellulose derived from seaweed presents benefits owing to its accessibility, rapid growth rate that does not require fertilizers, and non-competition with terrestrial food crops, making it a more sustainable resource [11,14]. Among the various types of seaweed explored, *Sargassum*, a brown macroalga abundant in tropical regions and often considered an environmental nuisance, remains underutilized despite its richness in polysaccharides.

The characteristics of cellulose fibers are significantly influenced by the extraction method and the chemicals employed during the treatment procedure [15]. A sequential chemical treatment was implemented in this study to extract and purify cellulose, which involved the use of Na<sub>2</sub>CO<sub>3</sub>, NaOH, and NaOCl. Na<sub>2</sub>CO<sub>3</sub> disrupts ionic interactions to facilitate the elimination of alginate, a distinctive component of brown seaweed; NaOH acts to depolymerize non-cellulosic components

<sup>&</sup>lt;sup>1</sup>Department of Metallurgical and Materials Engineering, Faculty of Engineering, Universitas Indonesia, Depok 16424, Indonesia

<sup>&</sup>lt;sup>2</sup>Research Center for Marine and Land Bioindustry, National Research and Innovation Agency, Tangerang Selatan 15314, Indonesia

<sup>&</sup>lt;sup>3</sup>Research Center for Biomass and Bioproduct, National Research and Innovation Agency, Cibinong 16911, Indonesia

<sup>&</sup>lt;sup>4</sup>Food and Technology Study Program, Faculty of Food Technology and Health, Sahid University, Jakarta 12870, Indonesia

<sup>&</sup>lt;sup>5</sup>Center for Sustainable and Waste Management, Universitas Indonesia, Depok 16424, Indonesia

and isolate cellulose fibers; and NaOCl serves as a bleaching agent to remove lignin and pigments [16].

Cellulose nanofibers (CNF) are a form of cellulose characterized by their tiny size, measured in nanometers, which confers a large surface area, exceptional mechanical strength, and significant water-binding capacity [17-18]. In contrast to Salem and Ismail [10], which used chemical hydrolysis to create CNF from seaweed, the current study focuses on mechanical degradation techniques. Previous work by Dilamian and Noroozi [19] reported fabricating CNF by combining high-pressure homogenization with a range of ultrasonication parameters, including time, power, and concentration. On the other hand, this study examines the impacts of homogenization, ultrasonication, and their combination as separate treatments. offering more comprehensive understanding of their individual and synergistic contributions to the morphology and crystallite profile of CNF. Morphological analysis is employed to investigate the surface structure of materials, inter-particle bonding strength, and structural changes after specific treatments [20]. While X-ray diffraction (XRD) complements this by effectively determining the cellulose crystallinity index, crystallite size, and cellulose classification.

Research on the extraction of CNF from *Sargassum* using a combination of chemical and mechanical treatments, particularly in relation to morphology and crystallinity, has not yet been reported. Therefore, this study aims to evaluate the morphology and crystallinity of CNF derived from *Sargassum* sp. These characterizations are expected to determine whether the applied treatments effectively produce clean, impurity-free fibers with suitable crystallinity properties for the use as functional materials in various applications, including biomedical fields. Nanocellulose, for instance, can function as a carrier in drug delivery systems, facilitating the controlled release of active substances within the body [21].

## EXPERIMENTAL SECTION

## **Materials**

The primary material used is *Sargassum* seaweed, obtained from Gunung Kidul, Yogyakarta. Prior to utilization, the seaweed was washed and sorted to

eliminate contaminants, including salt, sand, coral, and many other seaweed species. The washing procedure was conducted three times using clean water. The chemicals used are  $Na_2CO_3$ , NaOH, and NaOCl, which were purchased from Sigma Aldrich, USA.

#### Instrumentation

The instrumentations in this research were Fourier-transform infrared (Bruker Alpha II FTIR, Germany), XRD (Shimadzu 7000, Japan), scanning electron microscopy (SEM, Phenom Pro X), transmission electron microscopy (TEM, Talos F200C G2), analytical balance (Ohaus), hot plate stirrers (Biobase), pH indicator (Merck), glassware (Pyrex), and aluminum foil (Klinpak).

#### **Procedure**

## NFC preparation

A total of 100 g of *Sargassum* sp. was immersed in a 2%  $Na_2CO_3$  solution at 80 °C for 2 h. The solid was washed until neutral, then re-soaked in a 6% NaOH solution (1:20 w/v) at 80 °C for 2 h. A bleaching process was conducted using a 4% NaOCl solution (1:20 w/v) at 80 °C for 2 h. The solid was washed until neutral to obtain cellulose fiber. The moisture content of the cellulose fiber was then measured to determine the dry weight of the sample.

A 0.5% cellulose fiber suspension in distilled water was prepared and subjected to three types of mechanical treatment to produce CNF. The treatments were coded as follows: SCHBx for high-speed homogenization using a digital Ultra-Turrax (T25, IKA, Germany), SCHBy for ultrasonication using ultrasonic processors (VC750, Bioblock Scientific, France), and SCHBxy for the combination of both methods. The homogenization treatment was conducted at 10<sup>4</sup> rpm for 1 h, while ultrasonication was carried out for 30 min at 60% amplitude. The sample codes for the study are given in Table 1.

# Morphological analysis

The surface morphology and fiber structure at each stage were analyzed using SEM. The samples were placed on conductive carbon tape and coated with gold using a sputtering gold coater (Luxor).

| Tuble 1. Gode description |   |  |  |  |  |  |
|---------------------------|---|--|--|--|--|--|
| Sample codes              | Description   |  |  |  |  |  |
| S                         | Untreated Sargassum   |  |  |  |  |  |
| SC                        | Fibers after Na <sub>2</sub> CO <sub>3</sub> treatment                |  |  |  |  |  |
| SCH                       | Fibers after Na <sub>2</sub> CO <sub>3</sub> - NaOH treatment         |  |  |  |  |  |
| SCHB                      | Fibers after Na <sub>2</sub> CO <sub>3</sub> - NaOH - NaOCl treatment |  |  |  |  |  |
| SCHBx                     | Homogenization using Ultra-Turrax                                     |  |  |  |  |  |
| SCHBy                     | Ultrasonication using ultrasonic processor                            |  |  |  |  |  |
| SCHBxy                    | Combination of homogenization and ultrasonication                     |  |  |  |  |  |

Table 1. Code description

The fiber diameter was measured using TEM operated at a 200 kV accelerating voltage. A drop of 0.01 wt.% CNF suspension was placed on glow-discharged carbon TEM grids (200-mesh) blotted with filter paper and stained with 2% uranyl acetate to enhance contrast. The average diameter of cellulose nanofiber were calculated by ImageJ.

# Crystallographic analyses

Crystallographic analysis was performed using an XRD at a diffraction angle range of  $10^{\circ}$  to  $80^{\circ}$  with a scanning rate of  $2^{\circ}$ /min, utilizing Cu K $\alpha$  radiation ( $\lambda$  = 1.5418 Å), 40 kV voltage, and 30 mA current. The crystallinity index (CrI) of each sample was calculated using the diffraction intensities of the crystalline and amorphous regions based on the Segal method [22] in Eq. (1);

$$CrI(\%) = \frac{I_{200} - I_{am}}{I_{200}} \times 100\%$$
 (1)

where  $I_{200}$  is the maximum diffraction intensity of the crystalline lattice peak (at approximately  $2\theta = 22.7^{\circ}$ ), and  $I_{am}$  is the minimum intensity between the main peaks, representing the amorphous peak (at approximately  $2\theta = 18^{\circ}$ ).

Crystallite size (D) can be estimated using the Scherrer formula [23] in Eq. (2);

$$D = \frac{k\lambda}{\beta\cos\theta} \tag{2}$$

where k is the Scherrer constant (0.95);  $\lambda$  is the wavelength of the X-ray used;  $\beta$  is the true peak width at half maximum (FWHM) in radians of the peak considered; and  $\theta$  is the diffraction angle.

The Z function is used to determine the dominant crystalline structure, such as triclinic (I $\alpha$ ) and monoclinic (I $\beta$ ) allomorphs in cellulose I. This equation was developed

by Wada et al. [24] and is presented in Eq. (3); 
$$Z = 1693d_1 - 902d_2 - 549$$
 (3)

where  $d_1$  is the interplanar spacing (*d*-spacing) for lattice plane I $\alpha$  (100) or I $\beta$  (110),  $d_2$  is the interplanar spacing (*d*-spacing) for lattice plane I $\alpha$  (010) or I $\beta$  (110). If Z < 0, the cellulose I $\beta$  structure is the dominant form, and vice versa.

#### RESULTS AND DISCUSSION

## **Fibers from Multistep Preparation**

## Fiber morphology

Fig. 1 illustrates the surface of *Sargassum* fibers and the results of multistep preparation. Fig. 1(a) shows the surface of *Sargassum* fibers before treatment, which exhibits an interconnected fiber structure forming a dense network. This result is supported by research from Hii et al. [25], which states that *Sargassum* has an intact and dense structure, characteristic of both terrestrial plants and seaweed. The image also reveals the presence of small particles attached to the seaweed surface. These small particles are likely residual minerals remaining after the washing process. *Sargassum* grows attached to coral, so it is possible that coral fragments are still adhered to the holdfast (a root-like part that attaches to the substrate), making them difficult to remove through ordinary washing.

Fig. 1(b) shows the fiber morphology after alkaline treatment with Na<sub>2</sub>CO<sub>3</sub>. The fiber surface appears rough, but more uniform compared to the raw *Sargassum* fibers. Alkalinization with Na<sub>2</sub>CO<sub>3</sub> removes most of the noncellulose components, including alginate, which is one of the primary components of *Sargassum* [26-27]. Na<sub>2</sub>CO<sub>3</sub> dissolves alginate without damaging its structure, enabling further utilization of alginate. This treatment

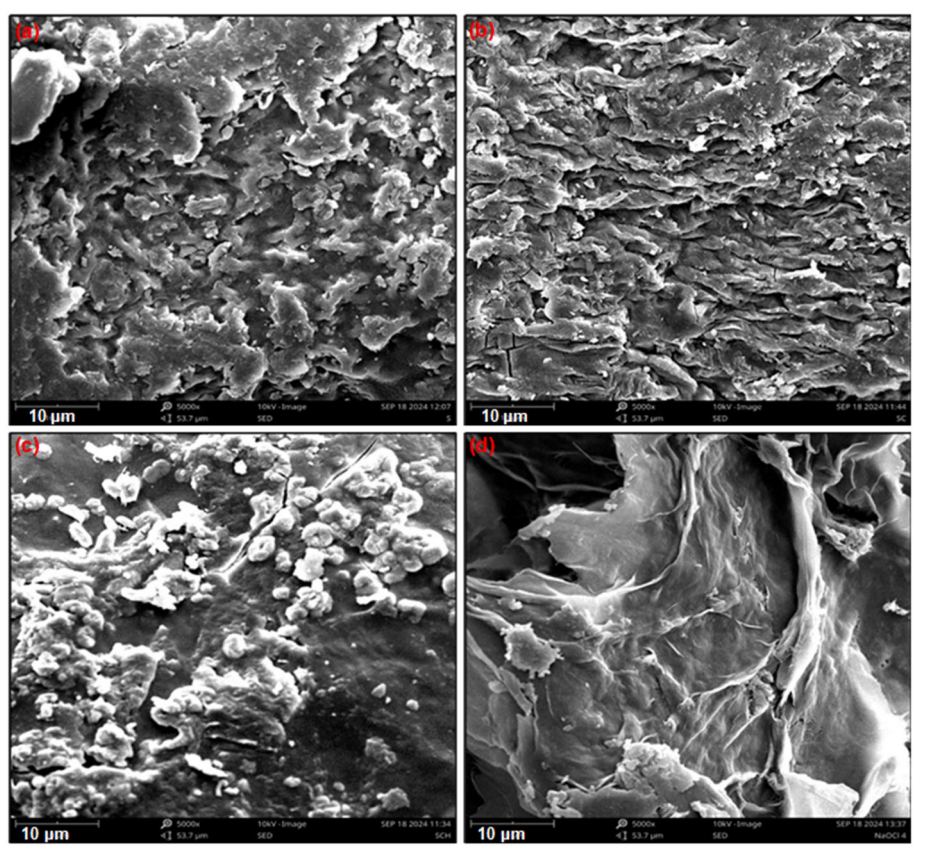


Fig 1. Morphology of multistep Sargassum fibers: (a) S, (b) SC, (c) SCH, and (d) SCHB

results in soft fibers resembling pulp, which, after drying, leads to a more uniform fiber structure. Fig. 1(c) presents the fiber morphology after alkalinization with Na<sub>2</sub>CO<sub>3</sub> and NaOH. The fibers appear cleaner and smoother due to the significant dissolution of hemicellulose and lignin. Additionally, the fiber length decreases, producing finer fibers. This finding is supported by Yuanita et al. [28], who reported that alkaline treatment can make fibers cleaner and smoother. Fig. 1(d) illustrates the fiber morphology after alkalinization followed by bleaching with NaOCl. The bleaching process aims to break down the lignin structure strongly bound to the fibers. As a result, the fiber morphology becomes smoother with enhanced visibility of pure cellulose fibers. The fiber length also decreases due to structural degradation, as reported by Ben Sghaier et al. [29].

# Crystalline fraction of fibers

The diffraction pattern of *Sargassum* and the fibers from multistep preparation can be seen in Fig. 2. In the diffractogram of untreated S, many overlapping peaks are

observed, with the two highest peaks at 14.5° and 22.7°, indicating the presence of amorphous components in the fibers. The broad and seemingly overlapping peaks are due to the mixture of various organic components in the seaweed, each with distinct diffraction patterns. Sundarrajan et al. reported that alginate has two

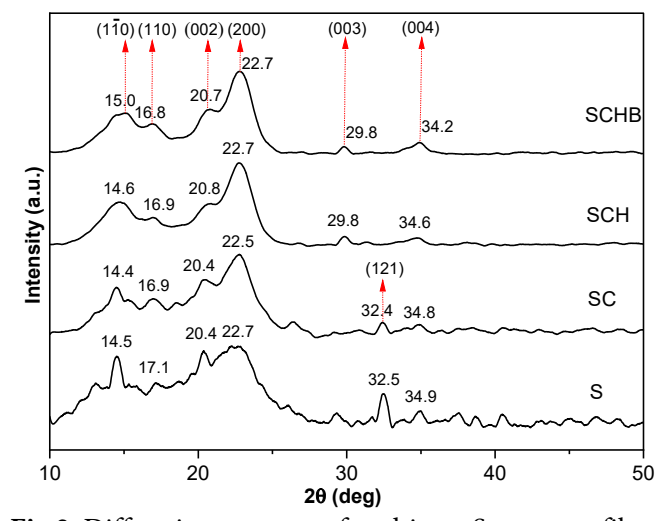


Fig 2. Diffraction patterns of multistep Sargassum fibers

characteristic peaks at diffraction angles of 14° and 22°, corresponding to polyguluronate (110)polymannuronate (200), respectively [30]. Meanwhile, Roziafanto et al. [31] also reported that the characteristic peaks of cellulose are found at diffraction angles of 15° and 22°. Therefore, these two peaks may represent a combination of alginate and cellulose contained in Sargassum. Additionally, numerous small peaks are observed, reflecting the heterogeneity of the internal structure and the presence of non-crystalline materials such as hemicellulose, lignin, or other impurities that may still be present in the raw material [28,32]. These impurities are likely inorganic minerals originating from sediments or coral remnants attached to the holdfast of the seaweed. Although the seaweed was washed and sorted to remove impurities prior to analysis, the parts adhering to the holdfast are difficult to separate through ordinary washing and are often still present in the sample.

This observation is supported by López-Sosa et al. [33], who reported that sharp peaks in the XRD diffractogram of Sargassum sp. samples correspond to minerals such as calcite (CaCO<sub>3</sub>) and dolomite (CaMg(CO<sub>3</sub>)<sub>2</sub>), which are commonly found in marine sediments. In addition to carbonates, marine sediments may contain SiO<sub>2</sub> and NaCl [34], which can accumulate on the seaweed surface during drying or post-harvest processing if the cleaning process is not optimal. SiO2 in marine sediment derives from terrestrial runoff and SiO<sub>2</sub>shelled marine organisms like diatoms, while NaCl is derived from seawater salinity. The lack of sharp and specific peaks indicates that the sample does not have a dominant crystalline phase. This could be due to the mixture of various organic components in the seaweed, each with distinct diffraction patterns. The diffraction pattern of Sargassum in this study exhibits more peaks compared to the report by Paniz et al. [35] on the brown seaweed species Cystosphaera jacquinotii. This difference may be attributed to insufficient washing of the sample, resulting in a higher presence of impurities, including coral remains and other contaminants.

Sharp and small peaks in the range of  $10^{\circ}-30^{\circ}$  are still visible but begin to decrease, indicating a reduction in impurities in SC. However, peak overlapping remains

noticeable. Immersing Sargassum in a Na<sub>2</sub>CO<sub>3</sub> solution reduces non-cellulose components such hemicellulose and protein [36-37]. The elimination of these amorphous components enhances crystallinity, resulting in a sharper peak at  $2\theta = 22.5^{\circ}$  compared to untreated samples. The XRD diffraction pattern of SCH shows a reduction in the intensity of minor peaks, indicating increased crystalline purity due to the removal of impurities in the advanced isolation process. The diffraction pattern displays two highest peaks observed at  $2\theta = 14.6^{\circ}$  and  $22.7^{\circ}$ , representing the  $(1\overline{1}0)$ and (200) planes, respectively, which are essential features of cellulose-based materials [31]. This indicates that NaOH effectively dissolves most lignin. The NaOH treatment degrades lignin, dissolving it in the alkaline solution, resulting in purer, cellulose-rich fibers [38].

The diffractograms of SCHB exhibit identical diffraction patterns, although there are changes in peak intensity and width, particularly at the primary 2θ angles of 15.0° and 22.7°. This indicates that SCH treatment effectively eliminated the majority of amorphous components, making the diffraction pattern similar to that of SCHB. These diffraction peaks are indicative of cellulose I allomorph [39]. Additionally, SCH and SCHB have no peaks at 32.4° unlike S and SC. Sahadat Hossain and Ahmed [40] reported that this diffraction angle corresponds to the aragonite phase of calcium carbonate with a (121) crystal plane, possibly originating from sediments or coral fragments associated with the *Sargassum* holdfast.

Table 2 shows the crystallinity index, crystallite size, and Z discriminant values of *Sargassum* and fibers obtained from multistep preparation. Based on calculations using the Segal method, the crystallinity index of *Sargassum* is 31.60%. This value indicates that the majority of its material structure is amorphous, approximately 69.40%. The low crystallinity level of this diffraction pattern suggests that *Sargassum* fibers contain a significant amount of amorphous compounds such as hemicellulose and lignin, resulting in low crystallinity. Preparation treatments through alkalization with Na<sub>2</sub>CO<sub>3</sub> increased the crystallinity index to 40.87% due to the removal of most non-cellulose components,

**Table 2.** Crystallinity index, crystallite size, and Z discriminant values of *Sargassum* and fibers from multistep preparation

| Treatments | Crystallinity index | Crystallite size (nm) |       |       |       |       |       | 7      |
|------------|---------------------|-----------------------|-------|-------|-------|-------|-------|--------|
| Treatments | (%)                 | $(1\bar{1}0)$         | (110) | (002) | (200) | (003) | (004) | L      |
| S          | 31.60               | 11.58                 | 13.46 | 8.35  | 3.70  | 14.80 | 14.18 | 258.39 |
| SC         | 40.87               | 6.12                  | 5.11  | 3.72  | 3.50  | 18.58 | 12.04 | 151.38 |
| SCH        | 59.17               | 3.34                  | 4.76  | 3.89  | 3.94  | 14.00 | 6.27  | 237.62 |
| SCHB       | 66.01               | 2.87                  | 4.90  | 5.07  | 3.94  | 0.60  | 8.95  | 159.99 |

such as alginate. Further treatment with NaOH treatment also increased the crystallinity index to 59.17% as hemicellulose and residual alginate from the previous treatment were reduced. Similarly, bleaching treatment further increased the crystallinity index to 66.01%. Thus, cellulose isolation with multistep preparation effectively enhances the CrI of the resulting fibers.

Crystallite size decreases additional with preparation steps, as shown in Table 2. The isolation process, particularly chemical treatments like alkalization and bleaching, plays a role in breaking hydrogen bonds between cellulose chains in the crystalline regions [41-42]. This bond-breaking loosens and fragments the crystalline structure, leading to smaller crystallite sizes. Furthermore, chemical treatments can also dissolve amorphous components like hemicellulose and lignin, which typically fill gaps between crystals [38]. The removal of these components increases the spacing between fibers, resulting in smaller observed crystallite sizes. This explains the trend in crystallite size observed in the samples, following the order SCHB < SCH < SC < S. Table 2 also shows the Z discriminant values for all treatments, which are positive. This indicates that the fibers obtained at each treatment stage are dominated by cellulose type Ia. These findings align with research by Thygesen et al. [43], which states that seaweed generally contains cellulose with type Ia structure as the dominant form. Type Ia cellulose is a triclinic structure commonly found in cellulose derived from algae and bacteria, differing from type Iβ, which is more often found in terrestrial plants [31].

## **Cellulose After Mechanical Treatment**

## Morphology of CNF

In this study, mechanical treatment was carried out through homogenization using Ultra-Turrax,

and a combination of both. ultrasonication, Morphological analysis using SEM showed that the resulting fibers had smooth surfaces. However, during the drying process, agglomeration occurred, forming sheet-like structures (Fig. 3). This phenomenon was also reported by Salem and Ismail [10]. Fig. 3(a) shows the morphology of cellulose fibers after the homogenization process using Ultra-Turrax. The fiber surfaces appear smooth but stacked, forming sheet-like structures. Ultra-Turrax works by applying a mechanical shear force to break down the fibers into smaller fibrils through friction and turbulence that is created by highspeed stirring blades. This process effectively reduces the initial particle size of the fibers into finer fibrils without causing significant damage to the fiber structure [44]. However, the intense friction and the inherently fibrous nature of cellulose can cause fibrils to reattach after homogenization, especially during the drying process, resulting in sheet-like layers.

The morphology of cellulose fibers after ultrasonication treatment is shown in Fig. 3(b). The surfaces of the fibers are also less rough than those of the fibers treated by homogenization, in agreement with previous investigations [19]. Ultrasonication employs high-frequency sound waves to generate pressure waves that create microbubbles in the solution. When these bubbles collapse, they produce extreme pressure and temperature, which can disrupt the fiber structure. It has been observed that ultrasonication treatment causes more severe degradation of the structural elements of the fibers, which become smoother and have a larger specific surface area [19].

The morphology of cellulose fibers treated with a combination of homogenization and ultrasonication is

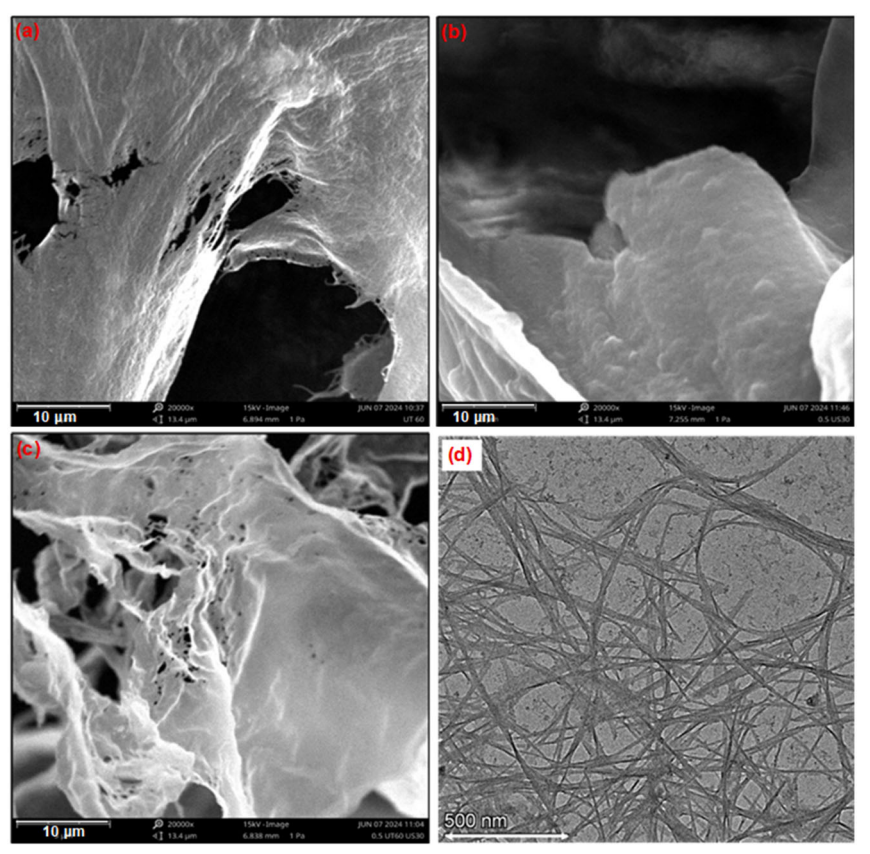


Fig 3. Morphology of cellulose fibers after mechanical treatment: (a) SCHBx, (b) SCHBy, and (c) SCHBxy, (d) TEM SCHBxy

shown in Fig. 3(c). This combined method aims to leverage the mechanical strength of Ultra-Turrax for initial particle size reduction, followed by ultrasonication to further break down the fibers, resulting in uniform fiber sizes and fine fibrils. The image (Fig. 3(c)) shows that the surface of the fibers treated with the combination of high-speed homogenization and ultrasonication appears smoother compared to other treatments. However, fiber diameter measurement could not be performed due to fiber overlapping caused by sample agglomeration during drying. Therefore, the fiber diameter was determined using TEM analysis, as shown in Fig. 3(d). The diameter measurement revealed an average fiber of 17.06 nm. This is consistent with the findings of Dilamian and Noroozi, who stated that the combination of homogenization and ultrasonication can produce nanofibers with diameters ranging from 6 to 20 nm [19].

# CNF crystallinity index

The diffraction patterns of cellulose after mechanical

treatment are shown in Fig. 4, revealing that all three treatments exhibit two main peaks with diffraction angles around 14° and 22°, corresponding to the (110) and (200) lattice planes, respectively. The sharpest and

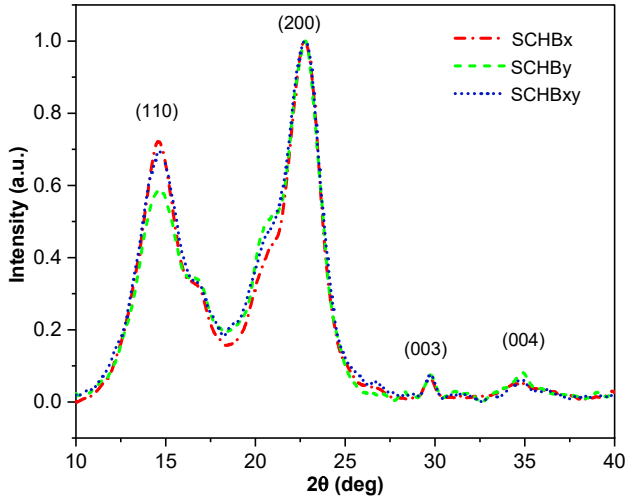


Fig 4. Diffraction patterns of cellulose after mechanical treatment

| • | •          | •                   |                       |       |       |       |       |       |        |
|---|------------|---------------------|-----------------------|-------|-------|-------|-------|-------|--------|
|   | Treatments | Crystallinity index | Crystallite size (nm) |       |       |       |       |       | 7      |
|   |            | (%)                 | (110)                 | (110) | (002) | (200) | (003) | (004) | L      |
|   | SCHBx      | 70.39               | 3.69                  | 7.18  | 3.82  | 4.09  | 13.99 | 6.28  | 209.82 |
|   | SCHBy      | 64.35               | 3.32                  | 6.57  | 4.20  | 3.90  | 16.37 | 9.25  | 209.82 |
|   | SCHBxv     | 66.88               | 3.41                  | 4.71  | 6.45  | 3.72  | 16.07 | 11.41 | 116.82 |

**Table 3.** Crystallinity index, crystallite size, and Z discriminant values of cellulose after mechanical treatment

highest peak is observed in the homogenization treatment using Ultra-Turrax, while the lowest peak is seen in the ultrasonication treatment.

The Ultra-Turrax operates with high shear forces, where the rotor spins at high speed within the solution, generating strong mechanical forces capable of breaking physical bonds between fibers. This method is more effective in dispersing and separating long nanocellulose fibers without damaging the crystalline structure of cellulose. In contrast, ultrasonication utilizes ultrasonic waves to create highly rapid and intense impact forces. These forces tend to break materials more aggressively, partially damaging the crystalline structure of cellulose. Ultrasonic waves induce depolymerization and reduce crystallinity by breaking parts of the crystalline structure into more amorphous regions [45].

Table 3 presents cellulose's crystallinity index, crystallite size, and Z discriminant values subjected to mechanical treatments. SCHBx has the highest crystallinity index at 70.39%, followed by SCHBxy at 66.88% and SCHBy at 64.35%. Ultra-Turrax provides strong mechanical forces primarily focused on fiber separation without damaging the crystalline structure, while ultrasonication uses more aggressive energy that can damage the crystalline structure, thereby reducing crystallinity [19,45-46]. The crystallite size in Table 3 indicates that the reduction in crystallite size is not uniform across all lattice planes. Cellulose has a crystalline structure consisting of various lattice planes, each with a different resistance to mechanical treatments [47]. Lattice planes with flatter orientations tend to have looser or fewer intermolecular bonds compared to sharper planes, making them easier to break. Meanwhile, the Z discriminant values are positive, indicating cellulose retains its type  $I\alpha$  structure. This suggests that mechanical treatments do not alter the structural type of cellulose but only reduce the fiber size.

#### CONCLUSION

The results show that cellulose fibers from *Sargassum* exhibit a type Ia structure with an increasing crystallinity index and decreasing crystallite size as the number of preparation stages increases during multistep preparation. Mechanical treatments applied to the resulting cellulose indicate that the combination of mechanical processes, such as homogenization and ultrasonication, produces smoother cellulose fibers with smaller sizes and more uniform size distribution.

# **■ ACKNOWLEDGMENTS**

This research was supported by the Seed Funding *Hibah Professor, Lektor Kepala, and Lektor* from the Faculty of Engineering, Universitas Indonesia, with grant number NKB-3461/UN2.F4.D/PPM.00.00/2024. The author also thank to National Research and Innovation Agency through *E-Layanan Sains*, for the scientific and technical support.

## **■ CONFLICT OF INTEREST**

The authors declare that they have no competing interests.

## AUTHOR CONTRIBUTIONS

Nurhayati conducted the conceptualization, collected the data, and writing - original draft, Hari Eko Irianto conducted the supervision and writing – review, Mochamad Chalid conducted the conceptualization and supervision, Rini Riastuti conducted the conceptualization and supervision. All authors agreed to the final version of this manuscript.

#### REFERENCES

[1] Ratna, R., Arahman, N., Munawar, A.A., and Aprilia,

- S., 2023, Extraction, isolation, and characterization of nanocrystalline cellulose from barangan banana (*Musa acuminata* L.) peduncles waste, *Indones. J. Chem.*, 23 (1), 73–89.
- [2] Baghel, R.S., Reddy, C.R.K., and Singh, R.P., 2021, Seaweed-based cellulose: Applications, and future perspectives, *Carbohydr. Polym.*, 267, 118241.
- [3] Zhang, W., Wang, X., Qi, X., Ren, L., and Qiang, T., 2018, Isolation and identification of a bacterial cellulose synthesizing strain from kombucha in different conditions: *Gluconacetobacter xylinus* ZHCJ618, *Food Sci. Biotechnol.*, 27 (3), 705–713.
- [4] Madhushree, M., Vairavel, P., Mahesha, G.T., and Bhat, K.S., 2024, A comprehensive review of cellulose and cellulose-based materials: Extraction, modification, and sustainable applications, *J. Nat. Fibers*, 21 (1), 2418357.
- [5] Doh, H., Dunno, K.D., and Whiteside, W.S., 2020, Cellulose nanocrystal effects on the biodegradability with alginate and crude seaweed extract nanocomposite films, *Food Biosci.*, 38, 100795.
- [6] He, Q., Wang, Q., Zhou, H., Ren, D., He, Y., Cong, H., and Wu, L., 2018, Highly crystalline cellulose from brown seaweed *Saccharina japonica*: Isolation, characterization and microcrystallization, *Cellulose*, 25 (10), 5523–5533.
- [7] Md Zaini, H.H., Mohammad-Noor, N., and Zainuddin, Z., 2021, Preliminary study on nanocellulose production in local seaweeds, *Int. STEM J.*, 2 (1), 36–42.
- [8] Siddhanta, A.K., Chhatbar, M.U., Mehta, G.K., Sanandiya, N.D., Kumar, S., Oza, M.D., Prasad, K., and Meena, R., 2011, The cellulose contents of Indian seaweeds, *J. Appl. Phycol.*, 23 (5), 919–923.
- [9] Wahlström, N., Edlund, U., Pavia, H., Toth, G., Jaworski, A., Pell, A.J., Choong, F.X., Shirani, H., Nilsson, K.P.R., and Richter-Dahlfors, A., 2020, Cellulose from the green macroalgae *Ulva lactuca*: Isolation, characterization, optotracing, and production of cellulose nanofibrils, *Cellulose*, 27 (7), 3707–3725.
- [10] Salem, D.M.S.A., and Ismail, M.M., 2022, Characterization of cellulose and cellulose

- nanofibers isolated from various seaweed species, *Egypt. J. Aquat. Res.*, 48 (4), 307–313.
- [11] Jmel, M.A., Anders, N., Ben Messaoud, G., Marzouki, M.N., Spiess, A., and Smaali, I., 2019, The stranded macroalga *Ulva lactuca* as a new alternative source of cellulose: Extraction, physicochemical and rheological characterization, *J. Cleaner Prod.*, 234, 1421–1427.
- [12] Chen, Y.W., Lee, H.V., Juan, J.C., and Phang, S.M., 2016, Production of new cellulose nanomaterial from red algae marine biomass *Gelidium elegans*, *Carbohydr. Polym.*, 151, 1210–1219.
- [13] Bogolitsyn, K., Parshina, A., and Aleshina, L., 2020, Structural features of brown algae cellulose, *Cellulose*, 27 (17), 9787–9800.
- [14] Gomaa, M., Al-Badaani, A.A., Hifney, A.F., and Adam, M.S., 2021, Industrial optimization of alkaline and bleaching conditions for cellulose extraction from the marine seaweed *Ulva lactuca*, *J. Appl. Phycol.*, 33 (6), 4093–4103.
- [15] Prakash Menon, M., Selvakumar, R., Suresh Kumar, P., and Ramakrishna, S., 2017, Extraction and modification of cellulose nanofibers derived from biomass for environmental application, *RSC Adv.*, 7 (68), 42750–42773.
- [16] Wang, T., and Zhao, Y., 2021, Optimization of bleaching process for cellulose extraction from apple and kale pomace and evaluation of their potentials as film forming materials, *Carbohydr. Polym.*, 253, 117225.
- [17] El-Ghoul, Y., Altuwayjiri, A.S., and Alharbi, G.A., 2024, Synthesis and characterization of new electrospun medical scaffold-based modified cellulose nanofiber and bioactive natural propolis for potential wound dressing applications, *RSC Adv.*, 14 (36), 26183–26197.
- [18] Yue, Y., Han, J., Han, G., French, A.D., Qi, Y., and Wu, Q., 2016, Cellulose nanofibers reinforced sodium alginate-polyvinyl alcohol hydrogels: Coreshell structure formation and property characterization, *Carbohydr. Polym.*, 147, 155–164.
- [19] Dilamian, M., and Noroozi, B., 2019, A combined homogenization-high intensity ultrasonication

- process for individualization of cellulose micro-nano fibers from rice straw, *Cellulose*, 26 (10), 5831–5849.
- [20] Chakraborty, I., Rongpipi, S., Govindaraju, I., Rakesh, B., Mal, S.S., Gomez, E.W., Gomez, E.D., Kalita, R.D., Nath, Y., and Mazumder, N., 2022, An insight into microscopy and analytical techniques for morphological, structural, chemical, and thermal characterization of cellulose, *Microsc. Res. Tech.*, 85 (5), 1990–2015.
- [21] Puppala, N.V., Doddipatla, P., and Mohannath, G., 2023, Use of nanocellulose in the intracellular delivery of biological and non-biological drugs: A review, *Cellulose*, 30 (3), 1335–1354.
- [22] Segal, L., Creely, J.J., Martin, A.E., and Conrad, C.M., 1959, An empirical method for estimating the degree of crystallinity of native cellulose using the X-ray diffractometer, *Text. Res. J.*, 29 (10), 786–794.
- [23] Nelson, M.L., and O'Connor, R.T., 1964, Relation of certain infrared bands to cellulose crystallinity and crystal lattice type. Part II. A new infrared ratio for estimation of crystallinity in celluloses I and II, *J. Appl. Polym. Sci.*, 8 (3), 1325–1341.
- [24] Wada, M., Okano, T., and Sugiyama, J., 2001, Allomorphs of native crystalline cellulose I evaluated by two equatorial *d*-spacings, *J. Wood Sci.*, 47 (2), 124–128.
- [25] Hii, S.L., Lip, K.F., Loh, Y.T., and Wong, C.L., 2015, Statistical optimization of fermentable sugar extraction from the Malaysian brown alga *Sargassum binderi*, *J. Appl. Phycol.*, 27 (5), 2089–2098.
- [26] Nogueira, M.T., Chica, L.R., Yamashita, C., Nunes, N.S.S., Moraes, I.C.F., Branco, C.C.Z., and Branco, I.G., 2022, Optimal conditions for alkaline treatment of alginate extraction from the brown seaweed *Sargassum cymosum* C. Agardh by response surface methodology, *Appl. Food Res.*, 2 (2), 100141.
- [27] Nesic, A., De Bonis, M.V., Dal Poggetto, G., Ruocco, G., and Santagata, G., 2023, Microwave assisted extraction of raw alginate as a sustainable and cost-effective method to treat beach-accumulated *Sargassum* algae, *Polymers*, 15 (14), 2979.
- [28] Yuanita, E., Pratama, J.N., Mustafa, J.H., and Chalid, M., 2015, Multistages preparation for microfibrillated

- celluloses based on *Arenga pinnata* "ijuk" fiber, *Procedia Chem.*, 16, 608–615.
- [29] Ben Sghaier, A.E.O., Chaabouni, Y., Msahli, S., and Sakli, F., 2012, Morphological and crystalline characterization of NaOH and NaOCl treated *Agave americana* L. fiber, *Ind. Crops Prod.*, 36 (1), 257–266.
- [30] Sundarrajan, P., Eswaran, P., Marimuthu, A., Subhadra, L.B., and Kannaiyan, P., 2012, One pot synthesis and characterization of alginate stabilized semiconductor nanoparticles, *Bull. Korean Chem. Soc.*, 33 (10), 3218–3224.
- [31] Roziafanto, A.N., Lazuardi, D.R., Ghozali, M., Sofyan, N., and Chalid, M., 2023, Hydrothermal treatment of sorghum (*Sorghum bicolor* (L.) Moench) stalks for enhanced microfibrillated cellulose production, *Mater. Res. Express*, 10 (9), 095303.
- [32] Nurhayati, N., Irianto, H.E., Riastuti, R., Pangesty, A.I., Nugraha, A.F., Todo, M., Chalid, M., and Jumahat, A., 2024, Extraction and characterization of micro-fibrillated cellulose from rice husk waste for biomedical purposes, *Int. J. Technol.*, 15 (2), 291–319.
- [33] López-Sosa, L.B., Alvarado-Flores, J.J., Corral-Huacuz, J.C., Aguilera-Mandujano, A., Rodríguez-Martínez, R.E., Guevara-Martínez, S.J., Alcaraz-Vera, J.V., Rutiaga-Quiñones, J.G., Zárate-Medina, J., Ávalos-Rodríguez, M.L., and Morales-Máximo, M., 2020, A prospective study of the exploitation of pelagic *Sargassum* spp. as a solid biofuel energy source, *Appl. Sci.*, 10 (23), 8706.
- [34] García-Rosales, G., Ordoñez-Regil, E., Ramírez Torres, J.J., López Monroy, J., Machain-Castillo, M.L., and Longoria-Gándara, L.C., 2011, Characterization of marine sediments using analytical techniques, *J. Radioanal. Nucl. Chem.*, 289 (2), 407–415.
- [35] Paniz, O.G., Pereira, C.M.P., Pacheco, B.S., Wolke, S.I., Maron, G.K., Mansilla, A., Colepicolo, P., Orlandi, M.O., Osorio, A.G., and Carreño, N.L.V., 2020, Cellulosic material obtained from Antarctic algae biomass, *Cellulose*, 27 (1), 113–126.
- [36] Dalal, S.R., Hussein, M.H., El-Naggar, N.E.A., Mostafa, S.I., and Shaaban-Dessuuki, S.A., 2021,

- Characterization of alginate extracted from *Sargassum latifolium* and its use in *Chlorella vulgaris* growth promotion and riboflavin drug delivery, *Sci. Rep.*, 11 (1), 16741.
- [37] Irianto, H.E., Giyatmi, G., Fransiska, D., and Nuraelah, A., 2023, Physical and chemical characteristics of alginate extracted from *Sargassum* sp, *IOP Conf. Ser.: Earth Environ. Sci.*, 1177 (1), 012029.
- [38] Mahdi, Y.S., Mohammed, A.H., and Mohammed, A.K., 2019, Cellulose fibers dissolution in alkaline solution, *Al-Khwarizmi Eng. J.*, 14 (2), 107–115.
- [39] French, A.D., 2014, Idealized powder diffraction patterns for cellulose polymorphs, *Cellulose*, 21 (2), 885–896.
- [40] Sahadat Hossain, M., and Ahmed, S., 2023, Crystallographic characterization of naturally occurring aragonite and calcite phase: Rietveld refinement, *J. Saudi Chem. Soc.*, 27 (3), 101649.
- [41] Romruen, O., Karbowiak, T., Tongdeesoontorn, W., Shiekh, K.A., and Rawdkuen, S., 2022, Extraction and characterization of cellulose from agricultural byproducts of Chiang Rai province, Thailand, *Polymers*, 14 (9), 1830.
- [42] Atiqah, M.S.N., Gopakumar, D.A., Owolabi, F.A.T., Pottathara, Y.B., Rizal, S., Aprilia, N.A.S., Hermawan, D., Paridah, M.T.T., Thomas, S., and Abdul Khalil, H.P.S., 2019, Extraction of cellulose nanofibers via eco-friendly supercritical carbon

- dioxide treatment followed by mild acid hydrolysis and the fabrication of cellulose nanopapers, *Polymers*, 11 (11), 1813.
- [43] Thygesen, A., Fernando, D., Ståhl, K., Daniel, G., Mensah, M., and Meyer, A.S., 2021, Cell wall configuration and ultrastructure of cellulose crystals in green seaweeds, *Cellulose*, 28 (5), 2763–2778.
- [44] Melo, A.R.A., Filho, J.C.D., Neto, R.P.C., Ferreira, W.S., Archanjo, B.S., Curti, R.V., and Tavares, M.I.B., 2020, Effect of ultra-turrax on nanocellulose produced by acid hydrolysis and modified by nano ZnO by sol-gel method, *Mater. Sci. Appl.*, 11 (2), 150–166.
- [45] Tonoli, G.H.D., Holtman, K.M., Glenn, G., Fonseca, A.S., Wood, D., Williams, T., Sa, V.A., Torres, L., Klamczynski, A., and Orts, W.J., 2016, Properties of cellulose micro/nanofibers obtained from eucalyptus pulp fiber treated with anaerobic digestate and high shear mixing, *Cellulose*, 23 (2), 1239–1256.
- [46] Chen, P., Yu, H., Liu, Y., Chen, W., Wang, X., and Ouyang, M., 2013, Concentration effects on the isolation and dynamic rheological behavior of cellulose nanofibers via ultrasonic processing, *Cellulose*, 20 (1), 149–157.
- [47] Ray, U., Zhu, S., Pang, Z., and Li, T., 2021, Mechanics design in cellulose-enabled high-performance functional materials, *Adv. Mater.*, 33 (28), 2002504.